The Effect of the Impedance Limit on the Reflection of Plane Waves in a Micropolar Thermoviscoelastic Material Using A Modified Green-Lindsay Model

Saurav SHARMA
University of Houston, 17900 Cambridge Street, #7-2G, Houston, Texas-77054, USA;
e-mail: sauravkuk@gmail.com

Abstract: - A new mathematical framework is used to look into how plane waves move through a micropolar thermoviscoelastic half-space using the modified Green-Lindsay (MG-L) generalized theory of thermoelasticity and impedance boundaries. With the right amounts, the controlling equations for the two-dimensional case become dimensionless. To make things even easier, the potential function method is used to separate the set of equations. The plane wave (longitudinal displacement (LD) wave, temperature (T) wave, coupled transverse displacement (CD I) wave, or coupled transverse microrotational (CD II) wave) hits the model, and four waves are reflected: LD, T, CD I, and CD II. For the impedance border, the amplitude ratios of these reflected waves are found compared to the wave that came in (LD or T or CD I or CD II). The amplitude ratios that are found depend on the frequency, the angle of incidence, and on the physical qualities of the medium. A graph shows how the factors of viscosity and impedance change the amplitude ratios. Due to this study, some special cases have been cut down. The results obtained can be used to develop new materials, which can be used to investigate coupled transverse and microrotation waves as well as coupled longitudinal and thermal waves.

Keywords: - micropolar thermoviscoelastic, modified Green-Lindsay, reflection, impedance factors, amplitude ratios.

1. INTRODUCTION

Engineering structures are often made of things that have a certain make-up inside. Included in this group are polycrystalline substances as well as those with a flexible or coarse grain structure. Classical elasticity is not enough to describe how this material behaves. The micropolar linear theory of elasticity is enough to describe how this kind of material behaves. The microstructure of the body has a big effect on brisk waves, which are high-frequency waves that have a short wavelength. These waves are caused by elastic shaking. Microstructure has an effect on elasticity that makes new types of waves appear that can't be seen in a standard linear theory of elasticity. A microstructure can be found in most natural and man-made materials, as well as in building, geology, and biology. Metals, polymers, dirt, rocks, and concrete are some other common things that have microstructure.

Eringen [2] and Eringen and Suhubi [1] came up with the linear theory of micropolar elasticity. People have come up with the linear theory of micropolar viscoelasticity [3, 4]. It was talked about how waves move through micropolar viscoelasticity and the growth equations that control this. The linear theory of micropolar thermoelasticity was created by adding temperature effects to the theory of micropolar continual [5]. This theory is called micropolar coupled thermoelasticity.

The concept of micropolar thermoelasticity and viscoelasticity, which is known as micropolar thermoviscoelasticity in the field of continuum mechanics.

Viscoelasticity looks at how a material reacts to changes in shape over time, while micropolar thermoelasticity checks how the material reacts to loads that are applied at high temperatures. In real-life engineering, micropolar thermoviscoelastic material is used in areas like aircraft and automotive where parts need to be able to handle changes in temperature and mechanical load over time.

Several writers have written about different kinds of issues that can arise in a micropolar thermoviscoelastic medium. Some of the most important ones are [6,7,8,9). Sharma and Kumar [10] presented plane waves analysis and fundamental solution thermoviscoelastic with voids. Sharma and Marin[11] explored the impact of two temperatures on the reflection of waves in micropolar realistic half space.

The Moore-Gibson-Thompson (MGT) model of thermoelasticity was used by Conti et al. [12] to show how to analyze a viscoelastic plate. The concept of thermoelasticity was employed by Marin et al. [13] to investigate a dipole fluid under a modified MGT by incorporating suitable initial conditions. Abouelregal and Sedighi [14] looked into what happens when the thermal conductivity changes in a yearly cylinder by using the MGT heat equation to build a

thermoviscoelastic model. Youssef and Al-Lehaibi [15] looked at how ramp-type thermal loading in a viscothermoelastic medium affected the shaking of a nanobeam with changing thermal conductivity. Marin et al. [16] employed fractional calculus with thermal relaxation periods to analyze a novel representation of the porothermoelastic model.

Abouelregal et al. [17] looked at the viscous stressed microbeam in the MGT heat equation when lasers heat it very quickly.

Sharma and Khator [18,19] examined some problems of power generation due to renewable sources and also explored micro-grid planning in the renewable inclusive prosumer market. Choudhary et al. [20] showed how plane waves are affected by non-local effects in a transversely isotropic viscothermoelastic material whose thermal conductivity changes. Sharma et al. [21] studied fundamental theorems and plane waves by using a novel mathematical formulation of temperature-dependent thermoelastic diffusion with multi-phase delays.

In acoustics, impedance is a way to measure how much a system blocks the flow of sound frequencies when sound waves are given to it. A lot of different areas, like earthquakes, geophysics, soil dynamics, seismology, and more, use the study of how seismic waves move through thermoviscoelastic media. The issue of plane waves reflecting off of things has been looked into in more than one way. Some of the notable works on the reflection of plane waves and Rayleigh waves under impedance boundary are listed in the kinds of literature [22,23,24,25].

Yu et al. [26] presented the Modified Green Lindsay (MG-L) theory of thermoelasticity. Kumar et al. [27] explored reflection problem in micropolar under the MG-L theory of thermoelasticity..

In this study, the reflection of plane waves in micropolar thermoviscoelastic by using the MG-L theory of thermoelasticity with impedance boundary has been investigated. The amplitude ratios of different reflected waves are obtained, such as the Longitudinal displacement (LD) wave, the Thermal (T) wave, the Coupled transverse (CD-I) wave, and the Coupled micro-rotational (CD-II) wave. The effects of viscosity and impedance parameters on amplitude ratios in micropolar under MG-L theory of thermoelasticity are figured out analytically and shown in the form of graphs.

2. BASIC EQUATIONS

After taking out the heat source, body forces, and body couple (Eringen [3,5] and Yu et al. [26]), the field equations and constitutive relations look like the following:

$$\left(1+\eta_1\tau_1\frac{\partial}{\partial t}\right)\left[(\lambda_0+\mu_0)\nabla(\nabla.\vec{u})+(\mu_0+K_0)\nabla^2\vec{u}+K_0\left(\nabla\times\vec{\phi}\right)\right]-\left(1+\eta_2\tau_1\frac{\partial}{\partial t}\right)\gamma_1\nabla T=\rho\frac{\partial^2\vec{u}}{\partial t^2},\quad(1)$$

$$\gamma_0\nabla^2\vec{\phi}+(\alpha_0+\beta_0)\nabla\left(\nabla.\vec{\phi}\right)+K_0\left[(\nabla\times\vec{u})-2\vec{\phi}\right]=\rho\hat{j}\frac{\partial^2\vec{\phi}}{\partial t^2},\quad(2)$$

$$K^*\nabla^2T=\rho C_e\left(1+\eta_3\tau_0\frac{\partial}{\partial t}\right)\frac{\partial T}{\partial t}+\left(1+\eta_4\tau_0\frac{\partial}{\partial t}\right)\gamma_1T_0\frac{\partial}{\partial t}\left(u_{r,r}\right),\quad(3)$$

$$t_{pq}=\left(1+\eta_1\tau_1\frac{\partial}{\partial t}\right)\left[\lambda_0u_{r,r}\delta_{pq}+\mu_0\left(u_{p,q}+u_{q,p}\right)+K_0\left(u_{q,p}-\varepsilon_{pqr}\phi_r\right)\right]-\gamma_1\left(1+\eta_2\tau_1\frac{\partial}{\partial t}\right)T\delta_{pq},\quad(4)$$

$$m_{pq}=\alpha_0\phi_{r,r}\delta_{pq}+\beta_0\phi_{p,q}+\gamma_0\phi_{q,p},\quad(5)$$

and

$$\lambda_0=\lambda\left(1+Q_1\frac{\partial}{\partial t}\right),\quad \mu_0=\mu\left(1+Q_2\frac{\partial}{\partial t}\right),\quad K_0=K\left(1+Q_3\frac{\partial}{\partial t}\right),\quad \alpha_0=\alpha\left(1+Q_4\frac{\partial}{\partial t}\right),$$

$$\beta_0=\beta\left(1+Q_5\frac{\partial}{\partial t}\right),\quad \gamma_0=\gamma\left(1+Q_6\frac{\partial}{\partial t}\right),$$

The numbers $(Q_1, Q_2, Q_3, Q_4, Q_5, Q_6)$ represent the micropolar viscoelastic relaxation times $=(\frac{\lambda^v}{\lambda},\frac{\mu^v}{\mu},\frac{K^v}{K},\frac{\alpha^v}{\alpha},\frac{\beta^v}{\beta},\frac{\gamma^v}{\gamma}$.

All the symbols are mentioned in the nomenclature.

The following cases come up:

(i) $\boldsymbol{\eta_1=\eta_2=\eta_3=\eta_4=1}$: for the Modified Green-Lindsay (MG-L) theory [26]**;**

(ii) $\boldsymbol{\eta_1=\eta_4=0,\ \eta_2=\eta_3=1}$:for the Green-Lindsay (G-L) theory [28];

(iii) $\boldsymbol{\eta_1=\eta_2=0,\ \eta_3=\eta_4=1}$:for the Lord-Shulman (L-S) theory [29];

(iv) $\boldsymbol{\eta_1=\eta_2=\eta_3=\eta_4=0}$: for the Coupled thermoelasticity theory [30];

3. PROBLEM FORMULATION

A homogeneous, isotropic, micropolar thermoviscoelastic half space within the frame work of the MG-L model, where $x_3 \geq 0$ and T_0 is the initial uniform temperature that has been considered. It is assumed that the rectangular Cartesian coordinate system (x_1, x_2, x_3) has an origin at the plane boundary $x_3= 0$ with the x_3-axis pointing normally into the medium as shown in Figure 1. Plane waves in the x_1-x_3 plane are considered such that the wave front is parallel to the x_2-axis, therefore, all the field variables are functions of x_1, x_3, and t. For the two-dimensional problem, the displacement vector and the micro-rotation vector are of the form

$$\vec{u} = (u_1, 0, u_3), \overrightarrow{\phi} = (0, \phi_2, 0), \quad (6)$$

Dimensionless quantities are taken as

$$(x_i', u_i') = \frac{\omega_1}{c_1}(x_i, u_i), \quad t_{3i}' = \frac{1}{\gamma_1 T_0} t_{3i},$$

$$T' = \frac{T}{T_0}, \ (t', \tau_0', \tau_1') = \omega_1(t, \tau_0, \tau_1),$$

$$\phi_2' = \frac{\rho c_1^2}{\gamma_1 T_0}\phi_2, \quad m_{32}' = \frac{\omega_1}{\gamma_1 c_1 T_0} m_{32},$$

$$(z_1', z_2') = \frac{c_1}{\gamma_1 T_0}(z_1, z_2), \ z_3' = \frac{{\omega_1}^2}{\rho {c_1}^3} z_3,$$

$$z_4' = \frac{c_1}{K^*} z_4 \quad (i = 1,3), \quad (7)$$

where

$$c_1^2 = \frac{\lambda + 2\mu + K}{\rho} \text{ and } \omega_1 = \frac{c_1^2 C_e \rho}{K^*}$$

Using (6) and (7) in (1) and (5) after turning off the primes lead to

$$\left(1 + \eta_1 \tau_1 \frac{\partial}{\partial t}\right)\left[b_1 \frac{\partial}{\partial x_1}\left(\frac{\partial u_1}{\partial x_1} + \frac{\partial u_3}{\partial x_3}\right) - b_3 \frac{\partial \phi_2}{\partial x_3} + b_2 \nabla^2 u_1\right] - b_4 \left(1 + \eta_2 \tau_1 \frac{\partial}{\partial t}\right)\frac{\partial T}{\partial x_1} = \frac{\partial^2 u_1}{\partial t^2}, \quad (8)$$

$$\left(1 + \eta_1 \tau_1 \frac{\partial}{\partial t}\right)\left[b_1 \frac{\partial}{\partial x_3}\left(\frac{\partial u_1}{\partial x_1} + \frac{\partial u_3}{\partial x_3}\right) + b_3 \frac{\partial \phi_2}{\partial x_1} + b_2 \nabla^2 u_3\right] - b_4 \left(1 + \eta_2 \tau_1 \frac{\partial}{\partial t}\right)\frac{\partial T}{\partial x_3} = \frac{\partial^2 u_3}{\partial t^2}, \quad (9)$$

$$b_5 \nabla^2 \phi_2 - b_6\left(\frac{\partial u_3}{\partial x_1} - \frac{\partial u_1}{\partial x_3}\right) - b_7 \phi_2 = \frac{\partial^2 \phi_2}{\partial t^2}, \quad (10)$$

$$\nabla^2 T = \left(1 + \eta_3 \tau_0 \frac{\partial}{\partial t}\right)\frac{\partial T}{\partial t} + b_8 \left(1 + \eta_4 \tau_0 \frac{\partial}{\partial t}\right)\frac{\partial}{\partial t}\left(\frac{\partial u_1}{\partial x_1} + \frac{\partial u_3}{\partial x_3}\right), \quad (11)$$

$$t_{33} = \left(1 + \eta_1 \tau_1 \frac{\partial}{\partial t}\right)\left(b_{12} \frac{\partial u_3}{\partial x_3} + b_{13} \frac{\partial u_1}{\partial x_1}\right) - \left(1 + \eta_2 \tau_1 \frac{\partial}{\partial t}\right) T, \quad (12)$$

$$t_{31} = \left(1 + \eta_1 \tau_1 \frac{\partial}{\partial t}\right)\left(b_9 \frac{\partial u_1}{\partial x_3} + b_{10} \frac{\partial u_3}{\partial x_1} - b_{11}\phi_2\right), \quad (13)$$

$$m_{32} = b_{14} \frac{\partial \phi_2}{\partial x_3}, \quad (14)$$

where b_i $(i = 1 \cdots 14)$ are given in Appendix I.

By introducing potential functions through Helmholtz decomposition, $u_1(x_1, x_3, t)$ and $u_3(x_1, x_3, t)$ can be expressed as

$$u_1 = \frac{\partial \psi_1}{\partial x_1} - \frac{\partial \psi_2}{\partial x_3}, u_3 = \frac{\partial \psi_2}{\partial x_1} + \frac{\partial \psi_1}{\partial x_3}, \quad (15)$$

Inserting equation (15) in equations (8)-(11) reduces to the following equations

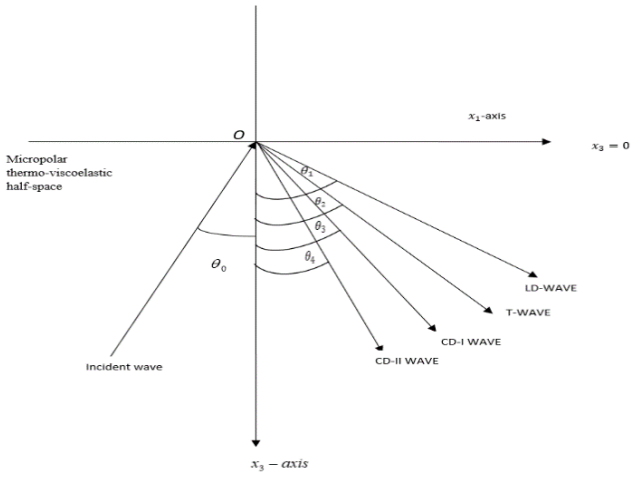

Figure 1. Schematic of the problem: incident and reflected waves for the incident wave at the boundary surface $x_3 = 0$

$$\left(1 + \eta_1 \tau_1 \frac{\partial}{\partial t}\right)\nabla^2 \psi_1 - b_4\left(1 + \eta_2 \tau_1 \frac{\partial}{\partial t}\right) T = \frac{\partial^2 \psi_1}{\partial t^2}, \quad (16)$$

$$\left(1 + \eta_1 \tau_1 \frac{\partial}{\partial t}\right)(b_2 \nabla^2 \psi_2 + b_3 \phi_2) = \frac{\partial^2 \psi_2}{\partial t^2}, \quad (17)$$

$$b_5 \nabla^2 \phi_2 - b_6 \nabla^2 \psi_2 - b_7 \phi_2 = \frac{\partial^2 \phi_2}{\partial t^2}, \quad (18)$$

$$\left(1 + \eta_3 \tau_0 \frac{\partial}{\partial t}\right)\frac{\partial T}{\partial t} + b_8\left(1 + \eta_4 \tau_0 \frac{\partial}{\partial t}\right)\frac{\partial}{\partial t}\nabla^2 \psi_1 = \nabla^2 T. \quad (19)$$

4. PLANE HARMONIC WAVE SOLUTIONS

Seeking, the plane harmonic solutions of equations (16) - (19) as

$$(\psi_1, T, \psi_2, \phi_2) = ({\psi_1}^o, T^o, \psi_2^o, {\phi_2}^o) e^{\iota\kappa(x_1 \sin\theta_0 - x_3 \cos\theta_0 + vt)}, \quad (20)$$

where ι is known as iota, κ denoted as wave number, and quantities such as ${\psi_1}^o, T^o, \psi_2^o, {\phi_2}^o$ are the constants representing the coefficients of the wave amplitudes, θ_0 is the angle of incidence.

By using the values of ψ_1, T, ψ_2, ϕ_2 from equation (20) in equations (16)-(19)determine the following equations:

$$(v^4 + E_{01} v^2 + E_{02})(\psi_1, T) = 0, \quad (21)$$

$$(v^4 + E_{03} v^2 + E_{04})(\psi_2, \phi_2) = 0, \quad (22)$$

where υ_i(i = 1,2) are roots of the characteristic equation $(\upsilon^4 + E_{01}\upsilon^2 + E_{02}) = 0$ and υ_j (j = 3, 4) are roots of the characteristic equation $(\upsilon^4 + E_{03}\upsilon^2 + E_{04}) = 0$. υ_1, υ_2, correspond to velocities of the LD-wave and T-wave in order of decreasing, whereas υ_3, υ_4 correspond to velocities of the CD-I wave and CD-II wave, decreasing from highest to lowest. Symbols are explained in Appendix II.

5. RESTRICTION ON BOUNDARY

The appropriate impedance boundary by following, Tiersten [31] and Malischewsky [32] at $x_3 = 0$ are

(i) $t_{33} + \omega z_1 u_3 = 0$,

(ii) $t_{31} + \omega z_2 u_1 = 0$,

(iii) $m_{32} + \omega z_3 \phi_2 = 0$,

(iv) $K^* \frac{\partial T}{\partial x_3} + \omega z_4 T = 0$, (23)

where z_1, z_2 are impedance parameters with dimensions Nsm^{-3}. The impedance parameters z_3 and z_4 are having dimensions Nsm^{-1} and $Nm^{-1}K^{-1}$ respectively.

Using the dimensionless quantities from equation (7), equation (23) becomes

(i) $t_{33} + \omega z_1 u_3 = 0$,

(ii) $t_{31} + \omega z_2 u_1 = 0$,

(iii) $m_{32} + \omega z_3 \phi_2 = 0$,

(iv) $\frac{\partial T}{\partial x_3} + \omega z_4 T = 0$, (24)

6. REFLECTION PHENOMENON OF WAVES

Taking the half-space surface $x_3 = 0$, that is subjected to impedance boundary with the x_3-axis pointing downward into the micropolar thermoviscoelastic medium. An incident wave makes an angle θ_0 with normal strikes the surface $x_3 = 0$ and four waves traveling in different directions with θ_1, θ_2, θ_3, and θ_4, the angle of reflection with the normal is reflected in the half-space as LD, T, CD-I, and CD-II waves. Figure 1 shows the complete geometry of the incident and reflected waves. The appropriate potentials in the half-space are read as

$$\psi_1 = \sum C_{0i}\, e^{\iota\kappa_0(x_1 \sin\theta_0 - x_3 \cos\theta_0) + \iota\omega t} + C_i e^{\iota\kappa_i(x_1 \sin\theta_i + x_3 \cos\theta_i) + \iota\omega t}, \quad (25)$$

$$T = \sum g_i \left(C_{0i} e^{\iota\kappa_0(x_1 \sin\theta_0 - x_3 \cos\theta_0) + \iota\omega t} + C_i e^{\iota\kappa_i(x_1 \sin\theta_i + x_3 \cos\theta_i) + \iota\omega t}\right), \quad (26)$$

$$\psi_2 = \sum D_{0i}\, e^{\iota\kappa_0(x_1 \sin\theta_0 - x_3 \cos\theta_0) + \iota\omega t} + D_i e^{\iota\kappa_j(x_1 \sin\theta_j + x_3 \cos\theta_j) + \iota\omega t}, \quad (27)$$

$$\phi_2 = \sum h_i \left(D_{0i} e^{\iota\kappa_0(x_1 \sin\theta_0 - x_3 \cos\theta_0) + \iota\omega t} + D_i e^{\iota\kappa_j(x_1 \sin\theta_j + x_3 \cos\theta_j) + \iota\omega t}\right), \quad (28)$$

where the coupling constants g_i and $h_i (i = 1 - 2)$ are defined in Appendix III. $C_{0i}(i = 1,2)$ stand for amplitude of incident LD-wave, T-wave and $D_{0i}(i = 1,2)$ display the amplitude of incident CD-I wave and CD-II wave. $C_i(i = 1,2)$ show the amplitude of the reflected LD-wave and reflected T-wave. $D_i(i = 1,2)$ correspond to the amplitude of the reflected CD-I wave and CD-II wave.

In order to achieve the appropriate boundary conditions, the Snell's Law extension is given by

$$\frac{\sin\theta_0}{\upsilon_0} = \frac{\sin\theta_i}{\upsilon_i} \quad (29)$$

where

$\kappa_i \upsilon_i = \omega$, at $x_3 = 0$ $(i = 1 \cdots 4)$,

$$\upsilon_0 = \begin{cases} \upsilon_1, & \text{incident LD} - \text{wave} \\ \upsilon_2, & \text{incident T} - \text{wave} \\ \upsilon_3, & \text{incident CD} - \text{I} - \text{wave} \\ \upsilon_4, & \text{incident CD} - \text{II} - \text{wave}, \end{cases}$$

Using the values of ψ_1, T, ψ_2 and ϕ_2 given by equations (25)–(28) in the boundary conditions given by equations (24) along with the equations (12)–(15) and equation (29), yield a linear system of equations as

$$\sum d_{ij} R_j = X_i, \qquad (i, j = 1 - 4), \quad (30)$$

where all d_{ij}, R_j and X_i are defined in Appendix IV.

7. SPECIFIC CASES

i) The amplitude ratios for the micropolar MG-L thermoviscoelastic half-space with thermal conducted impedance parameter are obtained by considering $z_1 = z_2 = z_3 = 0$ in (30).

ii) The results for micropolar thermoviscoelastic half-space under MG-L with tangential impedance parameter are figured out by taking $z_1 = z_3 = z_4 = 0$ in (30).

iii) The corresponding expressions for amplitude ratios are found for the micropolar MG-L get thermoviscoelastic half-space with tangential coupled

stress impedance parameter if $z_1 = z_2 = z_4 = 0$ in (30).

iv) The results are explored for the micropolar theory of thermoviscoelasticity under the L-S model by substituting $\eta_1 = \eta_2 = 0,\ \eta_3 = \eta_4 = 1$ in (30).

v) The results for micropolar thermoviscoelastic half-space under MG-L are determined when the impedance parameters z_1, z_2, z_3 and z_4 are not present in (30).

vi) The corresponding amplitude ratios for the micropolar theory of thermoviscoelasticity under the G-L model are attained by invoking the conditions $\eta_1 = \eta_4 = 0,\ \eta_2 = \eta_3 = 1$ in (30).

vii) The analogous amplitude ratios for micropolar MG-L thermoviscoelastic half-space with normal impedance parameters are procured by taking $z_2 = z_3 = z_4 = 0$ in (30).

8. NUMERICAL RESULT AND DISCUSSION

Taking an aluminium-epoxy material for numerical computation and the values of relevant physical constants are given by Gauthier [33],

$\lambda = 7.59 \times 10^{10}\mathrm{Nm}^{-2},\ \mu = 1.89 \times 10^{10}\mathrm{Nm}^{-2},$

$K = 0.0149 \times 10^{10}\mathrm{Nm}^{-2},$

$\gamma = 0.268 \times 10^{6}\mathrm{N},\quad \hat{j} = 0.001964\mathrm{m}^2,$

$C_e = 2.361 \times 10^{10}\mathrm{m}^2\mathrm{s}^{-2}\mathrm{K}^{-1}$

$\rho = 2.7 \times 10^{3}\ \mathrm{Kgm}^{-3},\ \omega = 0.2\mathrm{s}^{-1},$

$\alpha_t = 2.36 \times 10^{-6}\mathrm{K}^{-1},\ T_0 = 298\ \mathrm{K},$

$K^* = 0.492 \times 10^{2}\mathrm{Ns}^{-1}\mathrm{K}^{-1},\ \tau_0 = 0.2\mathrm{s}, \tau_1 = 0.4\mathrm{s}.$

The relevant parameters used for numerical computation can be expressed as

$Q_1 = .20\mathrm{s},\quad Q_2 = .15\mathrm{s},\quad Q_3 = .10\mathrm{s},$
$Q_6 = .5\mathrm{s}.$

The software MATLAB 7.10.4 has been used for numerical computation. The amplitude ratios of different reflected waves are plotted against the angle of incidence θ_0 for micropolar thermoviscoelastic MG-L model with the impedance parameters i.e. $z_1 = 1, z_2 = 5, z_3 = 2,\ z_4 = 3,$ without impedance parameters i.e. $z_1 = z_2 = z_3 = z_4 = 0,$ with viscosity parameters and without viscosity parameters.

For numerical illustration, we take the following:

I. Micropolar MG-L model with viscosity parameter and impedance parameters is represented by a solid line (VI).

II. Micropolar MG-L model with viscosity parameter and without impedance parameters is represented by the big dashed line (VWI).

III. Micropolar MG-L model without viscosity parameter and with impedance parameters is denoted by a solid line with center symbol diamond (◇) (WVI).

IV. Micropolar MG-L model without viscosity parameter and without impedance parameters is demonstrated by a big dashed line with center symbol circle (o) (WVWI).

8.1. Longitudinal Displacement-Wave

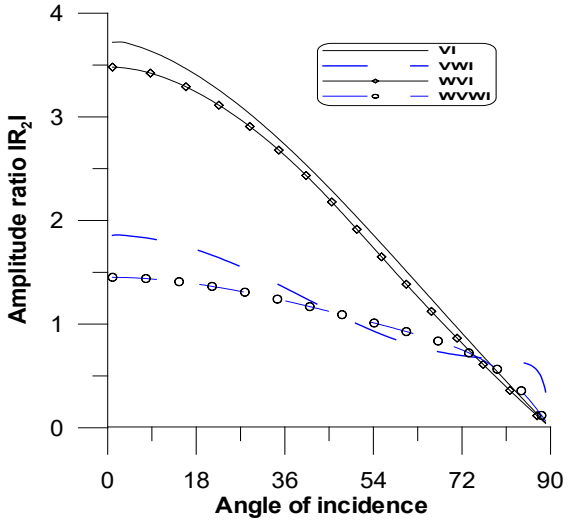

Figure 2. Variation of Amplitude ratio $|R_1|$ for LD wave

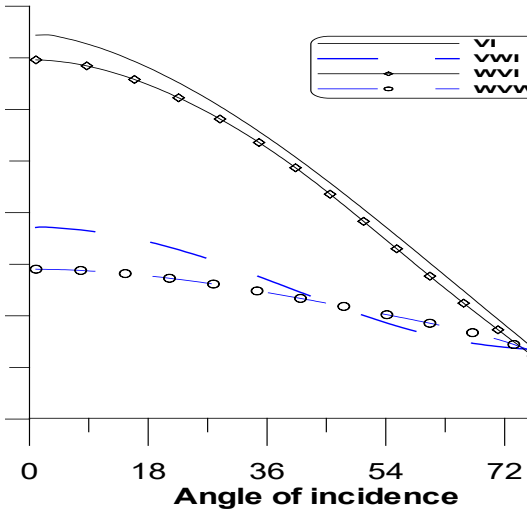

Figure 3. Variation of Amplitude ratio $|R_2|$ for LD wave

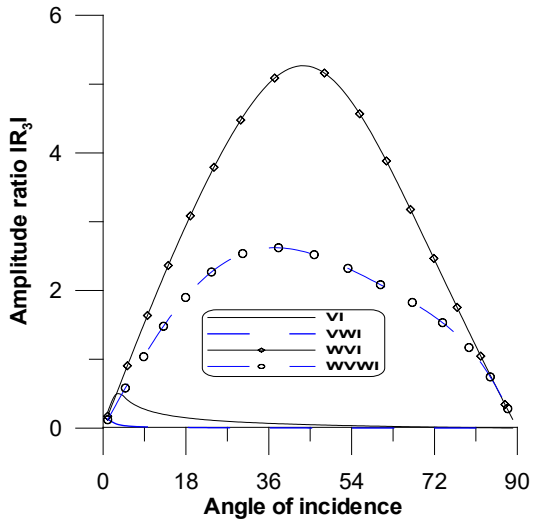

Figure 4. Variation of Amplitude ratio $|R_3|$ for LD wave

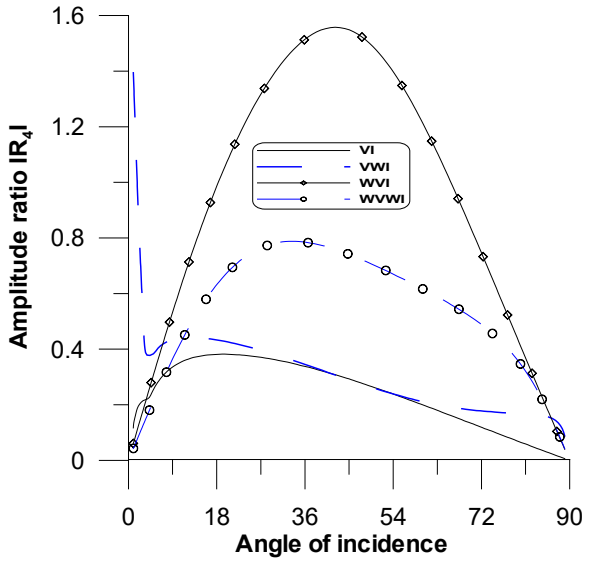

Figure 5. Variation of Amplitude ratio $|R_4|$ for LD wave

The variations of $|R_1|$ vs θ_0 are shown in figure 2. It is evident that the values of $|R_1|$ for VI and WVI are going in the opposite direction of VWI and WVWI across the whole range.

Figure 3 displays the variations of $|R_2|$ vs θ_0. It is noticed that the values of $|R_2|$ follow a descending trend for all the considered cases, but the magnitude of VI stays high as compared to other cases.

Figure 4 exhibits the variations of $|R_3|$ vs. θ_0. It is noticed that $|R_3|$ for WVI and WVWI follow an increasing trend in the first half of the interval and decrease for the rest of it. However, due to impedance parameters, the magnitude of $|R_3|$ for WVI to remain high. It is also been seen that $|R_3|$ for VI and VWI goes up near the boundary and down for the rest of the interval.

Figure 5 presents the variations of $|R_4|$ vs. θ_0. It is observed that $|R_4|$ for VI VWI behaves differently near the boundary and stays the same for the rest of the range. The values of $|R_4|$ depicts same trend for WVI and WVWI with significant difference in their magnitude.

8.2 Thermal-Wave

Figure 6 shows the variations of $|R_1|$ vs. θ_0. The magnitude of $|R_1|$ shows steady behaviour for VI, WVI, and WVWI, with a significant difference in their magnitudes whereas for VWI, the values of $|R_1|$ show small variations for the interval $0^o \leq \theta_0 \leq 45^o$ and show an increasing trend for rest of the period.

Figure 7 depicts the variations of $|R_2|$ vs. θ_0. It is noted that, the magnitude of $|R_2|$ drops sharply near the boundary for VI and VWI but stays the same behaviour in the left over the interval. It is also seen that the magnitude of $|R_2|$ follow similar trend for WVI and WVWI with considerable variance in their magnitude.

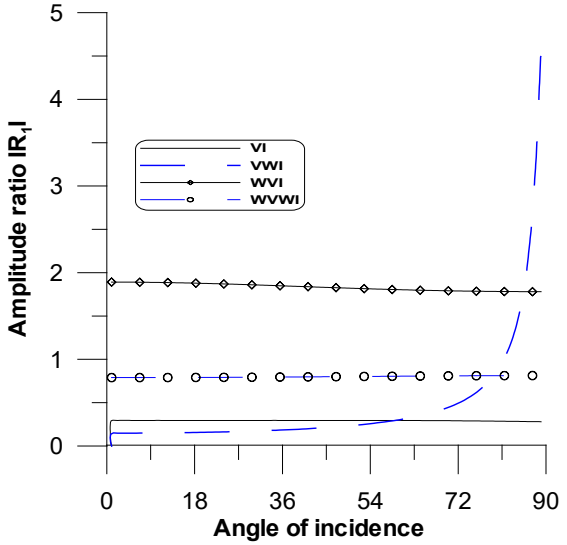

Figure 6. Variation of Amplitude ratio $|R_1|$ for T wave

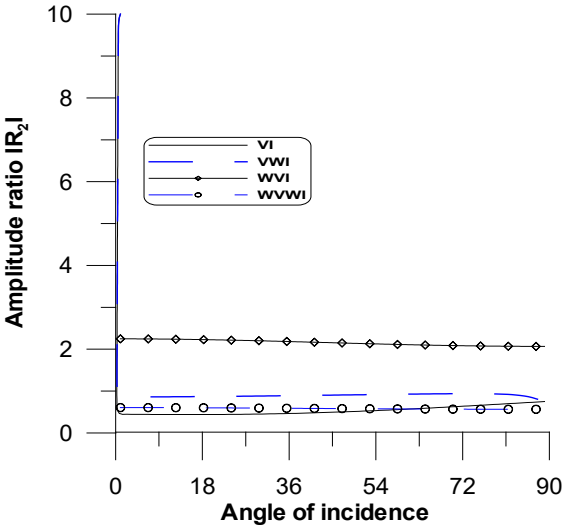

Figure 7. Variation of Amplitude ratio $|R_2|$ for T wave

Figure 8 demonstrates variations of $|R_3|$ vs θ_0. The magnitude of $|R_3|$ depicts an escalating trend for WVI and WVWI but the magnitude of WVI stays high because of impedance factors. Also, the magnitude of $|R_3|$ drops sharply near the boundary and then changes slightly around the origin for VI and VWI

Figure 9 depicts the variation of $|R_4|$ vs θ_0. The magnitude of $|R_4|$ shows an opposite trend near the boundary for VI and VWI when compared with WVI and WVWI and depicts the same trend for the rest of the interval for all considered cases.

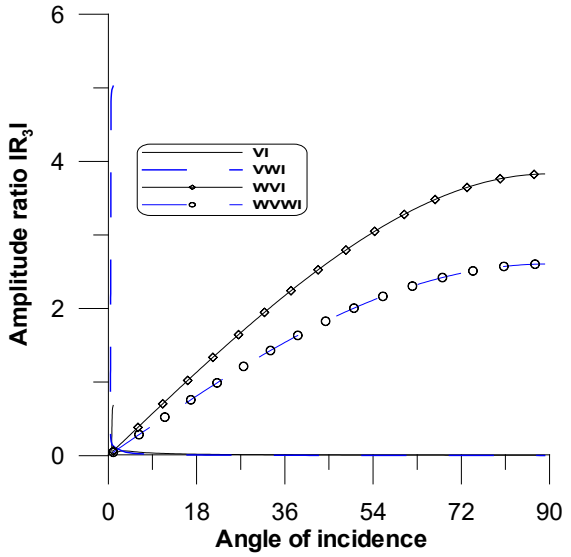

Figure 8. Variation of Amplitude ratio $|R_3|$ for T wave

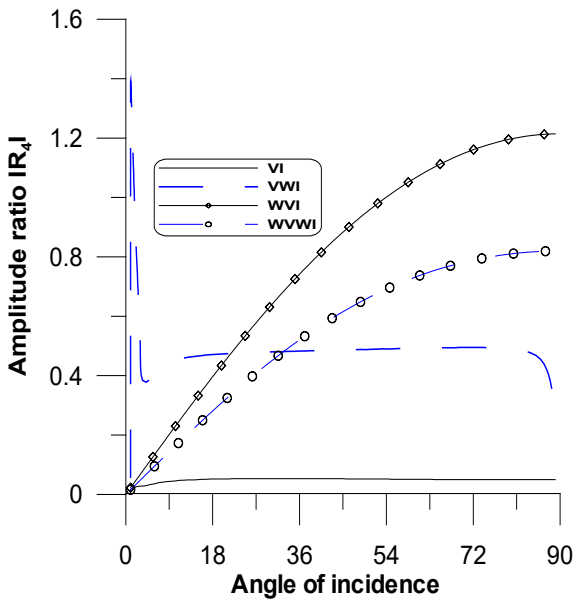

Figure 9. Variation of Amplitude ratio $|R_4|$ for T wave

8.3. CD I-Wave

Figure 10 depicts the variations of $|R_1|$ vs θ_0. When VI and WVI are close to the border, the value of $|R_1|$ goes up until it reaches its highest point at $\theta_0 = 36^o$, after that, it goes down for the rest of the interval. It is also noticed that $|R_1|$ goes up near and far away from the boundary and down for rest of the range in the case of VWI and WVWI.

Figure 11 demonstrates the trend of $|R_2|$ vs. θ_0. It is evident that the values of $|R_2|$ follow the same trend for all the considered cases with significant differences in their magnitudes.

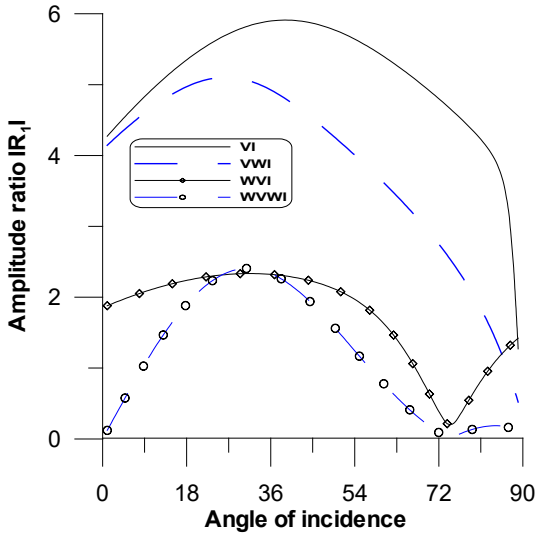

Figure 10. Variation of Amplitude ratio $|R_1|$ for CD I wave

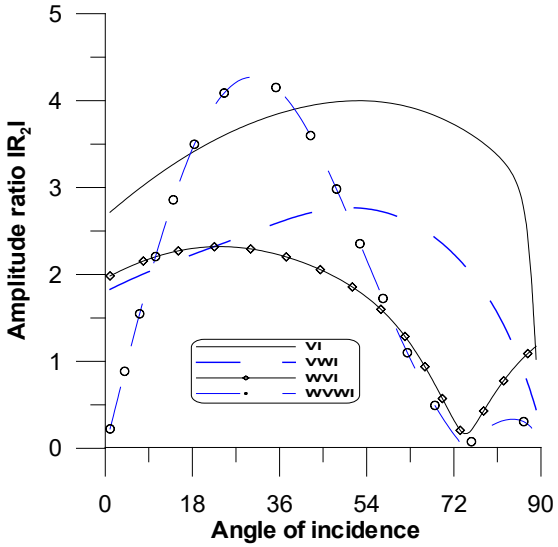

Figure 11. Variation of Amplitude ratio $|R_2|$ for CD I wave

Figure 12 depicts the variations of $|R_3|$ vs. θ_0. The magnitude of $|R_3|$ goes down for VWI and WVWI over the whole range whereas it but stays the same for

VI in the range $0^o \leq \theta_0 \leq 81^o$. After that, it goes down quickly for the rest of the range.

Figure 13 exhibits the trend of variations of $|R_4|$ vs. θ_0. It is claimed that $|R_4|$ shows a similar trend for VWI and WVI but due to the viscosity magnitude of $|R_4|$ stays high for VWI while it goes down in all the other cases.

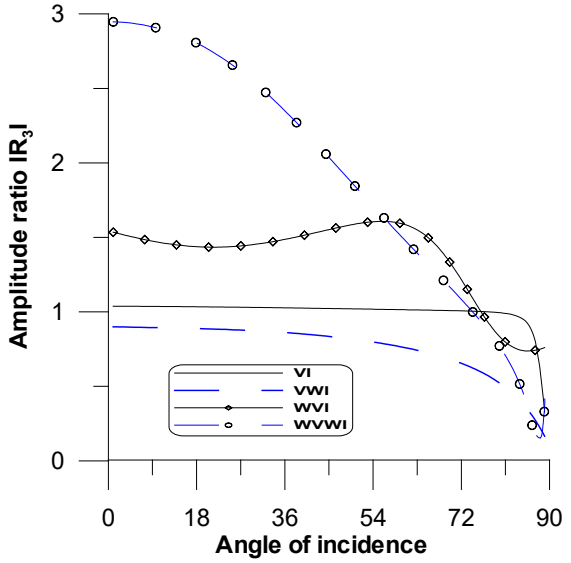

Figure 12. Variation of Amplitude ratio $|R_3|$ for CD I wave

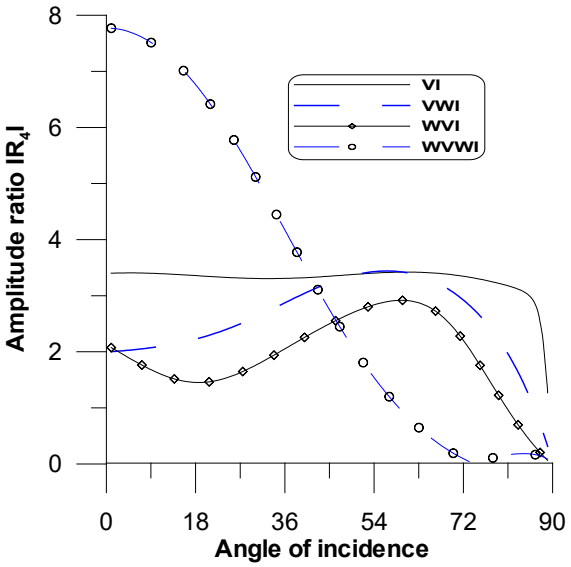

Figure 13. Variation of Amplitude ratio $|R_4|$ for CD I wave

8.4. CD II-Wave

Figure 14 displays variation of $|R_1|$ vs. θ_0. For values of $|R_1|$, the same pattern is observed for WVI and WVWI. However, because of impedance parameters, WVI stays large. Also $|R_1|$ shows an increasing trend for VWI and VI in the range $0^o \leq \theta_0 \leq 63^o$, while the remaining range shows an opposite trend.

Figure 15 shows the trend of $|R_2|$ vs. θ_0. It is noticed that $|R_2|$ goes down for VI and VWI but because of the effect of viscosity, the magnitude of $|R_2|$ stays high for VI. On the other hand, for WVI and WVWI, it goes up and then down for the whole range

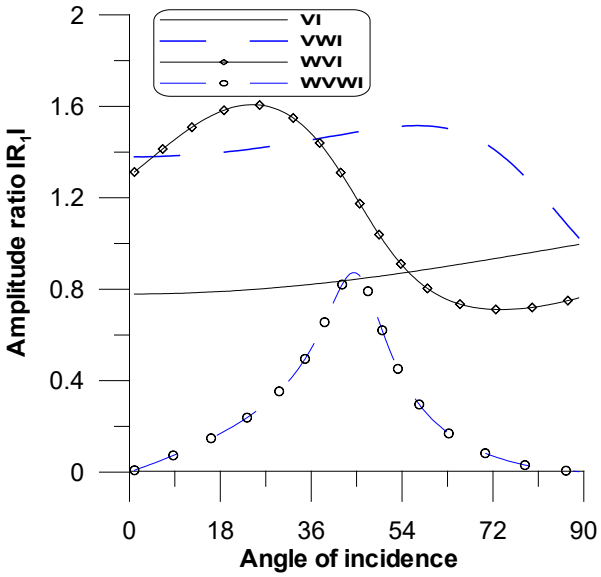

Figure 14. Variation of Amplitude ratio $|R_1|$ for CD II wave

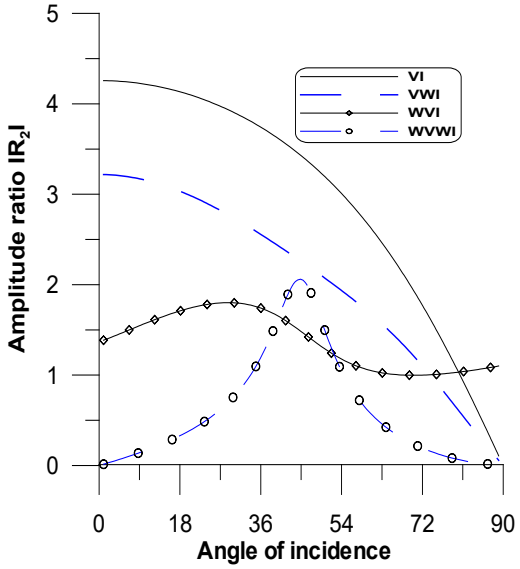

Figure 15. Variation of Amplitude ratio $|R_2|$ for CD II wave

The changes in $|R_3|$ with θ_0 . It can be seen that $|R_3|$ can be seen in Figure 16 moves in the opposite direction for WVI and WVWI between 0° and 36°, but it moves in the same direction for the rest of the interval. It has also been seen that $|R_3|$ shows an upward parabolic trend for both VI and VWI across the whole range.

Figure 17 shows a graph of $|R_4|$ vs. θ_0. In the first half of the interval, the value of $|R_4|$ shows an increasing trend in first half of the interval, goes up and peaks at $\theta_0 = 45^o$. As θ_0 goes up, the values of $|R_4|$ go down for VI and WVI but there is an oscillating trend for WVI and WVWI across the whole range.

VI and WVI behave in an alternating way between $0^o \leq \theta_0 \leq 54^o$. As θ_0 goes up, the values of $|R_4|$ stay pretty much the same, though there are big differences between them. On the other hand, VWI and WVWI go down over the whole range.

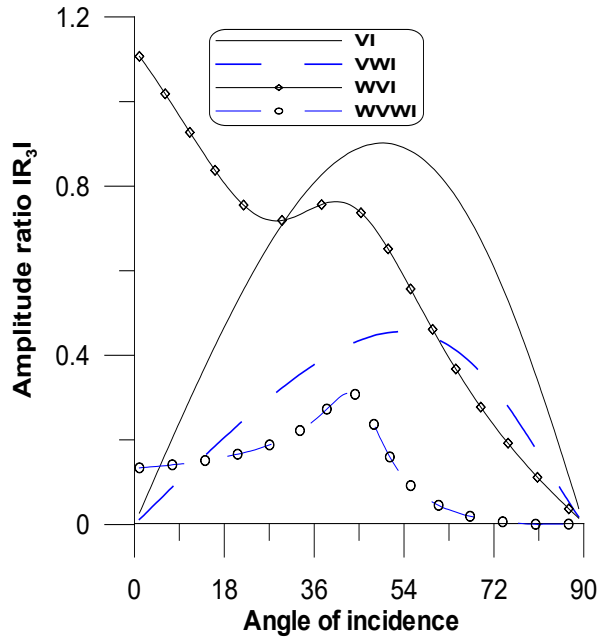

Figure 16. Variation of Amplitude ratio $|R_3|$ for CD II wave

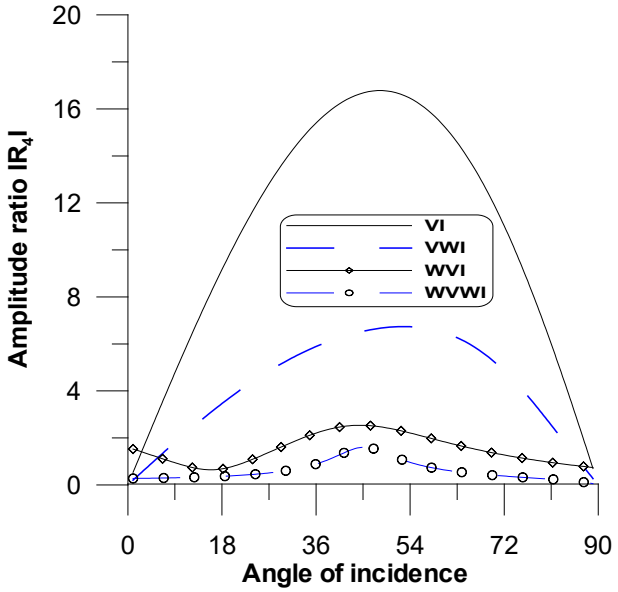

Figure 17. Variation of Amplitude ratio $|R_4|$ for CD II wave

9. CONCLUSION

This study investigates, how plane waves move and propagate in a micropolar thermoviscoelastic half space by employing the MG-L generalized theory of thermoelasticity along with an impedance boundary. The occurrence of an LD wave, a T wave, a CD-I wave, or a CD-II wave gives rise to amplitude ratios of different waves. Numbers are used to figure out these ratios, which show how viscosity and impendence factors affect the system. Based on the numerical results, the following conclusions are drawn.

(i) Through some values of θ_0, the impedance factors make the amplitude ratios of reflected LD, T, and CD-I waves bigger, but they make the amplitude ratios of reflected CD-II waves smaller. This takes place when an LD wave is incident.

(ii) When a T-wave is incident, the amplitude ratios of the reflected CD-I and CD-II waves go up, but the amplitude ratios of the reflected LD and T waves stay the same when viscosity factors are not taken into account.

(iii) When the CD-I wave is incident, the amplitude ratios of the reflected LD, T, and CD-I waves all go up, but the amplitude ratios of the CD-II wave go down in a limited range of incidence angles because of the viscosity factors.

(iv) Because of the viscosity factors, the amplitude ratios of reflected T, CD-I, and CD-II waves follow the same trend. However, the reflected LD wave follows the opposite trend when the CD-II wave is incident.

In conclusion, the viscosity and impedance factors have a big effect on the amplitude ratios. The problem is academic in nature, but the results can be used in geophysics and earthquake engineering. The finding in the numerical part might show a new way for waves to travel in a realistic model of the earth. Many seismological and exploring processes can be more effectively understood in light of this problem.

Appendix-I

$$b_1 = \frac{\lambda_0+\mu_0}{\rho c_1^2},\quad b_2 = \frac{\mu_0+K_0}{\rho c_1^2},\quad b_3 = \frac{K_0\gamma_1 T_0}{\rho^2 c_1^4},$$

$$b_4 = \frac{\gamma_1 T_0}{\rho c_1^2},\quad b_5 = \frac{\gamma_0}{\rho c_1^2 j},\quad b_6 = \frac{K_0 c_1^2}{j\gamma_1\omega_1^2 T_0},$$

$$b_7 = \frac{2K_0}{j\rho\omega_1^2},\quad b_8 = \frac{\gamma_1 c_1^2}{K^*\omega_1},\quad b_9 = \frac{\mu_0+K_0}{\gamma_1 T_0},$$

$$b_{10} = \frac{\mu_0}{\gamma_1 T_0},\quad b_{11} = \frac{K_0}{\rho c_1^2},\quad b_{12} = \frac{\rho c_1^2}{\gamma_1 T_0},$$

$$b_{13} = \frac{\lambda_0}{\gamma_1 T_0}, \quad b_{14} = \frac{\gamma_0 \omega_1^2}{\rho c_1^4}.$$

Appendix-II

$$E_{01} = \frac{\omega(\tau'_e \tau'_\theta + b_4 b_8 \tau'_f \tau'_g) - \iota}{\iota \tau'_e}, \; E_{02} = \frac{-\omega \tau'_\theta}{\iota \tau'_e},$$

$$E_{03} = \frac{-\omega^2 b_5 - \iota\omega \tau'_\theta(-b_2 b_7 + b_3 b_6 + b_2 \omega^2)}{\omega^2 - b_7},$$

$$E_{04} = \frac{b_2 b_5 \iota \omega^3 \tau'_\theta}{\omega^2 - b_7}, \tau'_\theta = \left(\tau_1 \eta_1 - \frac{\iota}{\omega}\right),$$

$$\tau'_e = \left(\tau_0 \eta_3 - \frac{\iota}{\omega}\right), \tau'_f = \left(\tau_1 \eta_2 - \frac{\iota}{\omega}\right),$$

$$\tau'_g = \left(\tau_0 \eta_4 - \frac{\iota}{\omega}\right).$$

Appendix-III

$$g_i = \frac{[\omega^2 - \omega \iota \kappa_i{}^2 \tau'_\theta]}{b_4 \omega \iota \tau'_f},$$

$$h_i = \frac{b_6 \kappa_j^2}{b_5 \kappa_j^2 + b_7 - \omega^2}, (i = 1,2), (j = 3,4).$$

Appendix-IV

$$d_{1p} = \iota \tau'_\theta \omega \left[b_{13} \sin^2\theta_p + b_{12} \cos^2\theta_p\right] \kappa_p^2 + \iota\omega\left[\tau'_f g_p - \kappa_p z_1 \cos\theta_p\right],$$

$$d_{1q} = -\iota\omega\kappa_q \left[\kappa_q (b_{13} - b_{12}) \tau'_\theta \sin\theta_q \cos\theta_q + z_1 \sin\theta_q\right],$$

$$d_{2p} = \iota\omega\kappa_p \left[\kappa_p (b_9 + b_{10}) \tau'_\theta \sin\theta_p \cos\theta_p - z_2 \sin\theta_p\right],$$

$$d_{2q} = \kappa_q^2 \iota \tau'_\theta \omega \left[-b_9 \cos^2\theta_q + 10_{10} \sin^2\theta_q\right] + \iota\omega\left[b_{11} h_p \tau'_\theta + \kappa_q z_2 \cos\theta_q\right],$$

$$d_{3q} = -h_p (b_{14} \iota \kappa_q \cos\theta_q + \omega z_3), \; d_{3p} = 0,$$

$$d_{4p} = -g_p \left[\iota \kappa_p \cos\theta_p + \omega z_4\right],$$

$$d_{4q} = 0, \quad , \; (p = 1,2), (q = 3,4),$$

where
R_1, R_2, R_3 and R_4 are the amplitude ratios of reflected LD-wave, reflected T-wave, CD-I wave, and CD-II wave making an angle $\theta_1, \theta_2, \theta_3$, and θ_4 as shown in figure 1 and are given by

$$R_1 = \frac{C_1}{B^*}, \quad R_2 = \frac{C_2}{B^*}, \quad R_3 = \frac{D_1}{B^*},$$

$$R_4 = \frac{D_2}{B^*},$$

For incident LD-wave,

$$B^* = C_{01} \text{ and } C_{02} = D_{01} = D_{02} = 0,$$

$$X_1 = -\iota\omega\tau'_\theta [b_{13} \sin^2\theta_0 + b_{12} \cos^2\theta_0] \kappa_0^2 - \iota\omega[\tau'_f g_1 + \kappa_0 z_1 \cos\theta_0],$$

$$X_2 = \iota\omega\kappa_0 [\kappa_0 (b_9 + b_{10}) \tau'_\theta \sin\theta_0 \cos\theta_0 + z_2 \sin\theta_0],$$

$$X_3 = 0,$$

$$X_4 = -g_1 [\iota\kappa_0 \cos\theta_0 - \omega z_4].$$

For incident T-wave,

$$B^* = C_{02} \text{ and } C_{01} = D_{01} = D_{02} = 0,$$

$$X_1 = -\iota\omega\tau'_\theta [b_{13} \sin^2\theta_0 + b_{12} \cos^2\theta_0] \kappa_0^2 - \iota\omega[\tau'_f g_2 + \kappa_0 z_1 \cos\theta_0],$$

$$X_2 = \iota\omega\kappa_0 [\kappa_0 (b_9 + b_{10}) \tau'_\theta \sin\theta_0 \cos\theta_0 + z_2 \sin\theta_0],$$

$$X_3 = 0,$$

$$X_4 = -g_2 [\iota\kappa_0 \cos\theta_0 - \omega z_4].$$

For incident CD I-wave,

$$B^* = D_{01} \text{ and } C_{01} = C_{02} = D_{02} = 0,$$

$$X_1 = -\iota\omega\kappa_0 [\kappa_0 (b_{13} - b_{12}) \tau'_\theta \sin\theta_0 \cos\theta_0 - z_1 \sin\theta_0],$$

$$X_2 = -\kappa_0^2 \iota\omega\tau'_\theta [-b_9 \cos^2\theta_0 + b_{10} \sin^2\theta_0] - \iota\omega[b_{11} h_1 \tau'_\theta - \kappa_0 z_2 \cos\theta_0],$$

$$X_3 = -(b_{14} \iota\kappa_0 \cos\theta_0 - \omega z_3) h_1,$$

$$X_4 = 0.$$

For incident CD II-wave,

$$B^* = D_{02} \text{ and } C_{01} = C_{02} = D_{01} = 0,$$

$$X_1 = -\iota\omega\kappa_0 [\kappa_0 (b_{13} - b_{12}) \tau'_\theta \sin\theta_0 \cos\theta_0 - z_1 \sin\theta_0],$$

$$X_2 = -\kappa_0^2 \iota\omega\tau'_\theta [-b_9 \cos^2\theta_0 + b_{10} \sin^2\theta_0] - \iota\omega[b_{11} h_2 \tau'_\theta - \kappa_0 z_2 \cos\theta_0],$$

$$X_3 = -(b_{14} \iota\kappa_0 \cos\theta_0 - \omega z_3) g_2,$$

$$X_4 = 0.$$

REFERENCES

[1] Eringen, A.C. and Suhubi, E.S., Non-linear theory of micro elastic solids I and II, Int. J. Eng. Sci. 2 (1964) 189–389.

[2] Eringen, A.C., Linear theory micropolar elasticity, J. Math. Mech. 15 (1966) 909–923.

[3] Eringen, A.C., Linear theory of micropolar viscoelasticity, Int. J. Eng. Sci. 5 (1967) 191–204.

[4] McCharty, M.F. and Eringen, A.C., Micropolar viscoelastic waves, Int. J. Eng. Sci. 7 (1969) 447–458.

[5] Eringen, A.C., Foundations of Micropolar Thermoelasticity, Course of Lectures, No. 23, CISM Udine, Springer, Berlin, 1970.

[6] Kanoria, M and Mallik, SH., Generalized thermoviscoelastic interaction due to periodically varying heat source with three phase-lag effect, Eur J Mech A/Solids., 29 (2010) 695–703.

[7] Mirzaei, M., Lord–Shulman nonlinear generalized thermoviscoelasticity of a strip, Int J Struct Stab Dynam, 20(2),2020, https://doi.org/10.1142/S0219455420500170.

[8] Ezzat, M.A., Fractional thermo-viscoelastic response of biological tissue with variable thermal material properties, J. Therm. Stresses, 43 (2020) 1120-1137.

[9] Abouelregal, A.E, Ahmad, H., Nofal, T.A. and Abu-Zinadah, H., Thermoviscoelastic fractional model of rotating nanobeams with variable thermal conductivity due to mechanical and thermal loads, Mod Phys Lett B, 22 (2021) 10.1142/s0217984921502973.

[10] Sharma, K., and Kumar,P., Propagation of plane waves and fundamental solution in thermoviscoelastic medium with voids, J. Therm. Stresses, 36(2) (2013)94-111.

[11] Sharma, K. and Marin, M.; Effect of distinct conductive and thermodynamic temperatures on the reflection of plane waves in micropolar elastic half-space, UPB Scientific Bulletin, Series A: Applied Mathematics and Physics, 75(2013),121-132.

[12] Conti, M., Pata, V. and Quintanilla, R., On the analyticity of the MGT –viscoelastic plate with heat conduction. Journal of Differential Equations, 269(10) (2020) 7862-7880.

[13] Marin, M. Öchsner, A. and Bhatti, M.M. ,Some results in Moore-Gibson-Thompson thermoelasticity of dipolar bodies, J. Appl.Math.Mech., (2020), 100(12), https://doi.org/10.1002/zamm.202000090.

[14] Abouelregal, A. E . and Sedighi HM, The effect of variable properties and rotation in a visco-thermoeastic orthopic annular cylinder under the Moore-Gibson-Thompson heat conduction model. Proceedings of the Institution of Mechanical Engineers, Part L: Jornal of Materials: Design and Applications. 235(5) (2021) 1004-1020.

[15] Youssef, H.M. and Al-Lehaibi, E.A.N., The vibration of a viscothermoelastic nanobeam of silicon nitride with variable thermal conductivity induced by ramp-type thermal loading. J. Therm Anal Calorim 146 (2021) 2387-2402.

[16] Marin, M., Hobiny, A. and Abbas, I.A., "The effects of fractional time derivatives in porothermoelastic materials using finite element method", Mathematics, (2021) 9, 1606. https://doi.org/10.3390/math9141606.

[17] Abouelregal, A.E., Ahmad, H., Badr, S., Almutairi, B. and Almohsen, B., Viscoelastic stressed microbeam analysis based on Moore-Gibson-Thompson heat equation and laser excitation resting on Winkler foundation. Journal of Low Frequency Noise Vibration and Active Control, 41, (2022), 1-22.

[18] Sharma, S. and Khator, S., Power generation planning with reserve dispatch and weather uncertainties including penetration of renewable sources. International Journal of Smart Grid and Clean Energy. (2021), doi: 10.12720/sgce.10.4.292-303.

[19] Sharma, S. and Khator, S., Micro-Grid planning with aggregator's role in the renewable inclusive prosumer market. Journal of Power and Energy Engineering. (2022), doi: 10.4236/jpee.2022.104004.

[20] Choudhary, S., Deswal, S. and Sheoran, S.S., Non-local impacts on planes waves in transversely isotropic viscothermoelastic medium with variable thermal conductivity. International Journal of Numerical Methods for Heat and Fluid Flow. 34(1), (2024) 109-130.

[21] Sharma, S., Devi, S., Kumar, R. and Marin, M. (2024), "Examining basic theorems and plane waves in the context of thermoelastic diffusion using a multi-phase-lag model with temperature dependence", Mechanics of Advanced Materials and Structures, https://doi.org/10.1080/15376494.2024.2370523.

[22] Singh, B., Yadav, A.K. and Kaushal, S., Effect of impedance boundary on reflection of plane waves from free surface of a rotating thermoelastic solid half space, Res J Eng Technol, 8(4), (2017), 405–413.

[23] Kumar, R., Singh, K, and Pathania, D.S., Propagation of Rayleigh waves in a micropolar thermoelastic half-space with impedance boundary conditions, Mat Phys Mech., 35 (2018), 115–125.

[24] Singh, B., Yadav, A.K. and Gupta, D., Reflection of plane waves from a micropolar thermoelastic solid half-space with impedance boundary conditions, J Ocean Eng Sci., 4 (2019), 122–131.

[25] Yadav, A.K., Carrera, E., Schnack, E., and Marin, M.; Effect of memory response and impedance barrier on reflection of plane waves in a nonlocal micropolar porous thermos-diffusive medium. Mechanics of Advanced Materials and Structures, doi: 10.1080/15376494.2023.2217556.

[26] Yu, Y.J., Xue, Z.N. and Tian, X.G., A modified Green-Lindsay thermoelasticity with strain rate to eliminate the discontinuity, Meccanica, 53, (2018), 2543-2554.

[27] Kumar,R., Kaushal,S. and Lal , A., Response of impedence parameters on waves in micropolar thermoelastic medium under modified Green -Lindsay theory.ZAMM,Journal of Applied Mathematics and Mechanics 102(9), 2022, 448-457, doi:10.1002/zamm.202200109.

[28] Green A. E. and Lindsay, K.A., Thermoelasticity, J.Elasticity, 2(1972), 1-7.

[29] Lord,H.W. and Shulman ,Y, ,A generalized dynamic theory of thermoelasticity, Journal of Mechanics and Physics of Solids,15(5), (1967), 299-303

[30] Dhaliwal,R.S. and Singh,A., Dynamic Coupled Thermoelasticity, Hinustan Publication Corporation, New Delhi, India, 1980

[31] Tiersten, H.F., Elastic surface waves guided by thin films, Journal of Applied Physics, 40, (1969), 770–789.

[32] Malischewsky, P.G., Surface waves and discontinuities, Elsevier 1987, Amsterdam.

[33] Gauthier, R.D., Experimental Investigations on Micropolar Media, Mechanics of Micropolar Media, (1982), 395–463, https://doi.org/10.1142/9789812797247_0007.